CHAPTER 4

GaN Laser Diodes on Nonpolar and Semipolar Planes

K. M. Kelchner,* **S. P. DenBaars,*,†** and **J. S. Speck†**

Contents

* Department of Electrical and Computer Engineering, University of California, Santa Barbara, CA, USA
† Materials Department, University of California, Santa Barbara, CA, USA

Semiconductors and Semimetals, Volume 86
ISSN 0080-8784, DOI: 10.1016/B978-0-12-391066-0.00004-6

1. INTRODUCTION

GaN and its alloys with Al and In are remarkably well suited for optical applications spanning a large portion of the electromagnetic spectrum from deep ultraviolet, through the visible, and into the infrared. With direct bandgaps ranging from 0.65 eV for InN to 3.4 eV for GaN to 6.2 eV for AlN, (Al,Ga,In)N-based emitters are the leading contender for solving the ''green gap'' problem, a span of wavelengths from approximately 500–600 nm (green through yellow) that have historically shown severely low-output efficiency by any other semiconductor emitter. In the 1990s, progress on (Al,Ga,In)N devices competed with high interest in II–VI compound semiconductors such as ZnSe for violet, blue, and green light-emitting diode (LED) and laser diode (LD) applications. These II–VI emitters, however, often suffered from poor performance due to poor lifetimes, poor stability, and poor reliability. While the GaN material system offered improved characteristics for both electronic and optical applications, some major developmental roadblocks hindered initial progress. These early obstacles related to crystal growth and material quality, specifically, high-defect densities on lattice-mismatched substrates (see Section 3.1) and difficulties realizing *p*-GaN conductivity (as described by Nakamura *et al*., 2000).

Nakamura *et al*. demonstrated the first electrically injected GaN LD in 1996. At the time, it was the shortest wavelength semiconductor LD ever reported at 417 nm. Since this initial demonstration only 16 years ago, GaN-based violet LDs have seen fantastic commercial success as the light source for high-definition video and high-density data storage technology known as Blu-Ray. The short wavelength of the violet 405 nm InGaN-based laser source allows at least 5–10 times higher data capacity compared to standard DVD technologies. Only a few years since the first Blu-Ray readers and discs were available commercially, GaN LD technology has continued to improve and higher power violet lasers can now write to four-layer discs capable of storing 128 GB of data (Pioneer, 2010). Other applications of violet and near ultra-violet lasers currently undergoing product development include medical imaging, laser-based printing, UV curing, water purification, and biodetection.

In the past few years, researchers are pushing the capabilities of GaN-based emitters toward longer visible wavelengths, into the blue and green spectrums. GaN-based blue LEDs combined with yellow-emitting phosphors can generate white light and are integral components for general solid-state-based illumination. LDs in the blue and green spectral regions are likewise integral components in laser-based lighting applications such as red–green–blue (RGB) or red–yellow–green–blue (RYGB) full-color backlit displays, heads-up displays, and projectors. For these applications, LDs offer directional, spectrally pure, focus-free light, and a wider

color gamut compared to LEDs. LDs also offer smaller size, less energy consumption, increased speed, and longer lifetimes compared to traditional bulb-based light sources. To realize RGB or RYGB displays requires three to four separate LD sources. Efficient, direct-emission red AlGaInP lasers have been available for many years. Indirect or synthetic green LDs based on second harmonic generation of 1060–1064nm LDs have also been available commercially. However, nitride-based direct-emission blue and green LDs offer reduced cost, reduced form factors, and increased efficiency and reliability.

GaN LDs in the blue spectrum (near 450nm) finally hit the markets in 2007 (Nichia, 2007) and are just beginning to be employed as blue sources in laser-based displays. The first commercially available direct-emission green nitride LDs (520nm) are poised to hit the market in 2011, (Nichia, 2010; Optics, 2010) making purely direct-emission laser displays realizable for the first time. This technology milestone has enormous potential for integrating small, low-power consumption, portable projectors in next-generation cell phones and digital cameras in addition to laser-based television displays and highly directional laser-based lighting applications.

While GaN is closing in on the green gap and could see immediate implementation in a variety of display applications, there have still been several challenges toward achieving GaN LDs much beyond 450nm. These longer wavelengths require high-indium concentration in InGaN quantum well (QW) active regions, which can be difficult both from a growth and materials perspective, particularly on the most commonly used basal *c*-plane GaN which is limited by built-in polarization, discussed in Section 2.1. The longest wavelength GaN LDs grown on the basal plane still have lower output powers and wall-plug efficiencies (WPE, a ratio of optical power out over the input current and voltage) compared to LDs in the pure blue spectrum: approximately one-tenth the output power (80mW compared to 800mW) and one-fourth WPE of (5–6% compared to 20%), as reported by Lutgen *et al.* (2011).

Orientations of GaN other than the standard basal plane have some very desirable properties that may make them a better choice for solving the green gap problem, the most important of which is the reduction or elimination of built-in polarization field that plagues polar *c*-plane InGaN devices as well as increased material gain. The first violet LDs on non-basal orientations of GaN were demonstrated simultaneously by UCSB (Schmidt *et al.*, 2007b) and Rohm (Okamoto *et al.*, 2007a) in 2007 on *m*-plane $(10\bar{1}0)$ GaN plane, 11 years after the first *c*-plane LD demonstration. The first semipolar LD was demonstrated by Tyagi *et al.* (2007) on free-standing $(10\bar{1}\bar{1})$ later that year. Despite the relatively late start in the race toward achieving lasing in the green wavelengths, LDs on nonpolar and semipolar planes have seen rapid improvements rivaling the best results on *c*-plane, particularly at wavelengths in the blue and green, as

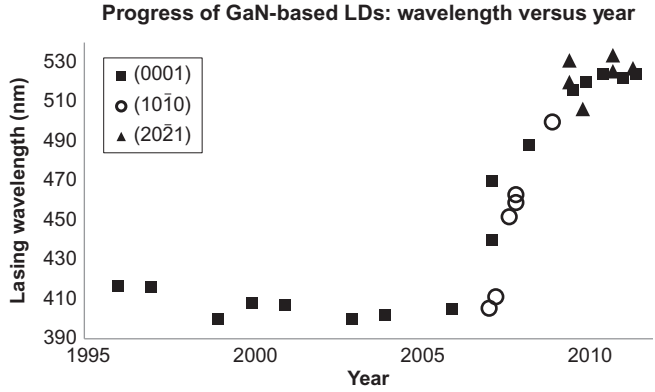

FIGURE 4.1 Summary of progress of GaN LDs shown as wavelength versus year for *c*-plane, semipolar $(20\bar{2}1)$ plane and nonpolar *m*-plane, from the first GaN LDs to the present. Data taken from the following references: For *c*-plane: Nakamura *et al.* (1996), Nakamura *et al.* (1997), Asano *et al.* (1999), Takeya *et al.* (2000), Miyajima *et al.* (2001), Asano *et al.* (2003), Ito *et al.* (2004), Nam *et al.* (2006), Schwarz *et al.* (2007), Miyoshi *et al.* (2008), Avramescu *et al.* (2009), Lutgen *et al.* (2010), Avramescu *et al.* (2010), Lutgen *et al.* (2011), and Zhang *et al.* (2011); For nonpolar *m*-plane: Schmidt *et al.* (2007b), Feezell *et al.* (2007), Okamoto *et al.* (2007a,b), Kubota *et al.* (2008), Tsuda *et al.* (2008), and Okamoto *et al.* (2009). For semipolar $(20\bar{2}1)$: Tyagi *et al.* (2009), Enya *et al.* (2009), Adachi *et al.* (2010) and Kim *et al.* (2011).

shown in the summary of evolution of wavelength with time in Fig. 4.1. Soraa recently demonstrated state-of-the art blue and green LDs using unspecified nonbasal planes of GaN, citing some of the highest WPE reported for single-mode blue LDs at 23% (Raring *et al.*, 2010). Sumitomo Electric demonstrated the first purely green (above 520nm) LDs on a semipolar $(20\bar{2}1)$ plane in 2010, and at the time of writing, currently holds the record for longest wavelength GaN-based LD ever reported at 533.6nm (Adachi *et al.*, 2010).

The rest of this chapter outlines several key properties of GaN LDs on these alternative crystal planes and discusses how these properties influence the design of LD devices emitting in the visible spectrum.

2. MATERIAL PROPERTIES OF DIFFERENT PLANES OF GaN

2.1. Polarization

Hexagonal wurtzite (WZ) GaN is the most thermodynamically stable crystal structure of GaN and the basal *c*-plane (0001) is the most commonly used crystal orientation, as it is easily grown on (0001) sapphire or

(0001) SiC. Each group-III atom is tetrahedrally coordinated to four nitrogen atoms, arranged in an ABABAB stacking sequence, where A and B refer to Ga–N atomic bilayers. WZ GaN (space group $P6_3mc$ and point group 6mm) is noncentrosymmetric, meaning it lacks inversion symmetry, yielding large built-in spontaneous polarization P_{sp} in the [0001] *c*-direction. The values for spontaneous polarization for (Al,In,Ga)N materials are nearly one-third the values for typical perovskite ferroelectrics such as $BaTiO_3$ (Speck and Chichibu, 2009).

Stemming from the lattice mismatch of InN and GaN, InGaN QWs grown pseudomorphically on GaN substrates will become elastically strained as long as it is below the critical thickness for plastic relaxation. For *c*-plane GaN, this is a biaxially compressive stress that induces an additional piezoelectric polarization on the order of 1MV/cm (Sala *et al.*, 1999). For QW structures, the discontinuities in polarization cause a build-up of sheet charges at the interfaces, producing an electric field that bends the energy bands, as illustrated in Fig. 4.2. This band bending directs the electron and hole wave functions in opposite directions, and the resulting spatial separation of confined carriers can reduce oscillator strength and recombination rates (Im *et al.*, 1998). Additionally, the band bending reduces the transition energy of the bound states which can red-shift the emission wavelength. This effect, the quantum-confined Stark effect (QCSE), can have deleterious effects on optoelectronic devices and worsens for QWs with higher indium compositions due to increased lattice mismatch, making it particularly detrimental for higher-wavelength applications.

An additional side effect of the internal fields of *c*-plane GaN light emitters is the emission peaks that will gradually blue-shift with

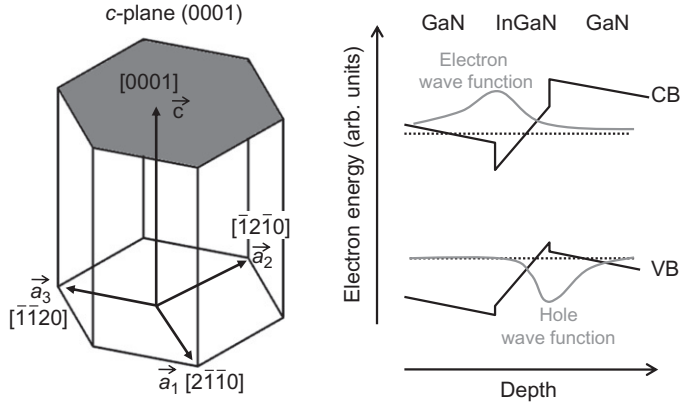

FIGURE 4.2 (A) The *c*-plane of wurtzite GaN structure, and (B) Approximation of band-bending effects and resulting wave function separation due to polarization discontinuities.

increasing current densities, due to gradual Coulomb screening of the polarization-related internal electric fields. For high current densities required for LDs (above 1kA/cm^2 and sometimes as high as 10kA/cm^2), this blue-shift of wavelength can be quite significant, requiring even higher indium compositions to realize the target wavelength. Minimizing the blue-shift with current density can be possible by increasing the number of wells, which should reduce the effective carrier density in each well (Peter *et al.*, 2008). Additionally, stronger polarization fields in the active region may act as potential barriers for carrier transport, which can result in high-operating voltage (Lutgen *et al.*, 2010; Queren *et al.*, 2009a,b). To avoid these problems, QWs grown on polar *c*-plane GaN are generally limited to less than 3nm in width.

There are several symmetric *nonpolar* crystal planes that occur several times in the WZ unit cell, orthogonal to the basal plane. Because of their crystal symmetry, the nonpolar *a*-planes $\{11\bar{2}0\}$ and *m*-planes $\{10\bar{1}0\}$ have zero inherent spontaneous polarization. Further, InGaN QWs grown on nonpolar GaN orientations do not induce any polarization discontinuities or suffer from any strain-induced piezoelectric polarization effects along to the growth direction. For QWs grown on nonpolar crystal orientations, the energy bands remain flat, as shown in the Fig. 4.3. Because there are no spatial separation of electron and hole wavefunctions, the wavefunction overlap is essentially unity.

The effect of improved overlap and the absence of piezoelectric polarization were demonstrated in some of the earliest nonpolar films, showing a ten to one hundred times reduced decay times for *m*-plane

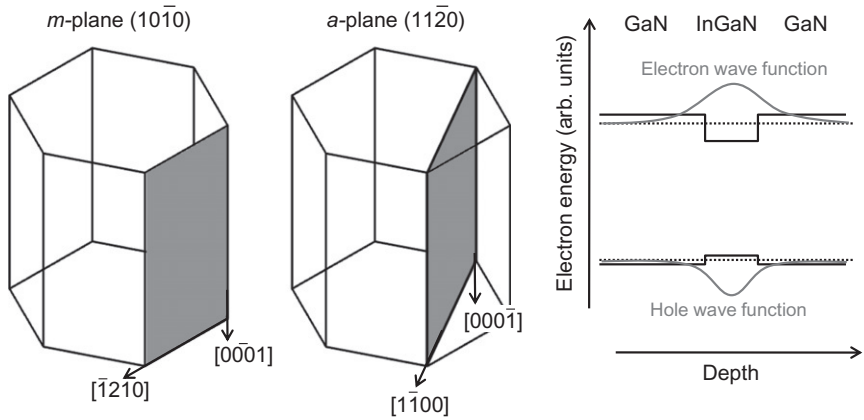

FIGURE 4.3 Nonpolar (A) *m*-plane and (B) *a*-plane of wurtzite GaN, (C) Flat band conditions due to lack of polarization discontinuities, overlap of electron and hole wavefunctions.

compared to *c*-plane QWs (Waltereit *et al.*, 2000) and high brightness photoluminescence (PL) from nonpolar MQWs (Sun *et al.*, 2003). Only a few years after the demonstration of the first *a*-plane (Chen *et al.*, 2003) and *m*-plane LEDs (Chakraborty *et al.*, 2005b; Gardner *et al.*, 2005), UCSB demonstrated violet *m*-plane LEDs on low-defect density bulk substrates with comparable device performance to state-of-the-art *c*-plane devices (Schmidt *et al.*, 2007a). (Early reports showed more stable performance and higher output powers observed for LEDs grown on bulk *m*-plane substrates compared to *a*-plane, which is why this orientation is generally preferred (Yamada *et al.*, 2008a).) Subsequent studies of nonpolar LEDs continued to demonstrate smaller blue-shifts with current density even up to blue-green wavelengths (Lin *et al.*, 2009a), and lower efficiency droop compared to *c*-plane (Ling *et al.*, 2010), attributed more uniform carrier injection. (It is important to also note that nonpolar emitters show some blue-shift of wavelength, which is frequently attributed to other effects such as band filling of localized states at potential minima of the QW plane (Chichibu, 1996).) The absence of the QCSE of nonpolar QWs can also permit growth of wider QWs without a significant loss in radiative efficiency, particularly for QWs of high crystal quality and low indium composition (Kim *et al.*, 2007a). This finding hugely benefits LD optical waveguiding design, discussed further in Section 4.2.

There are a number of additional planes with a nonzero *h*, or *k*, or *i* and a nonzero *l* Miller-Bravais indices that can also serve as growth surfaces (Baker *et al.*, 2005). Since these mixed index planes have a *c*-axis component in their normal direction, they have *some* spontaneous polarization (Takeuchi *et al.*, 2000) and are collectively referred to as *semipolar* planes. The strength of the total polarization and the polarization discontinuity between strained InGaN layers and GaN substrate depends on both the angle from *c*-plane and the composition of the InGaN layer. Romanov *et al.* (2006) calculated polarization discontinuities along the growth direction for strained InGaN films on GaN planes inclined at arbitrary angles from the *c*-plane, recreated in Fig. 4.4. There is a crossover point of zero polarization for planes oriented around 45° from the *c*-plane due to the angular dependence (with respect to the *c*-plane) of the sign and magnitude of strain components and their impact on polarization through the piezoelectric coefficients.

The first semipolar LED was demonstrated on $(30\bar{3}8)$ sapphire (inclined 54.7° from *c*-plane) (Kamiyama *et al.*, 2005), followed by demonstrations on $(10\bar{1}1)$ (inclined 62° from *c*-plane) and $(10\bar{1}3)$ planes (Chakraborty *et al.*, 2005a), all demonstrating reduced blue-shift with current density and confirming reduced polarizations compared to *c*-plane devices. Over the past several years, semipolar LEDs and LDs have been explored on a variety of planes, including $(11\bar{2}2)$, $(10\bar{1}1)$, and $(20\bar{2}1)$ (oriented 58°, 62°, and 75° from *c*-plane, respectively, as shown in

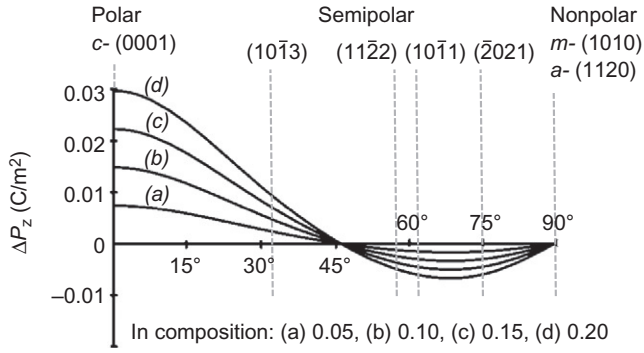

FIGURE 4.4 Polarization discontinuity for planes of GaN oriented at arbitrary angles from *c*-axis, after Romanov *et al.* (2006).

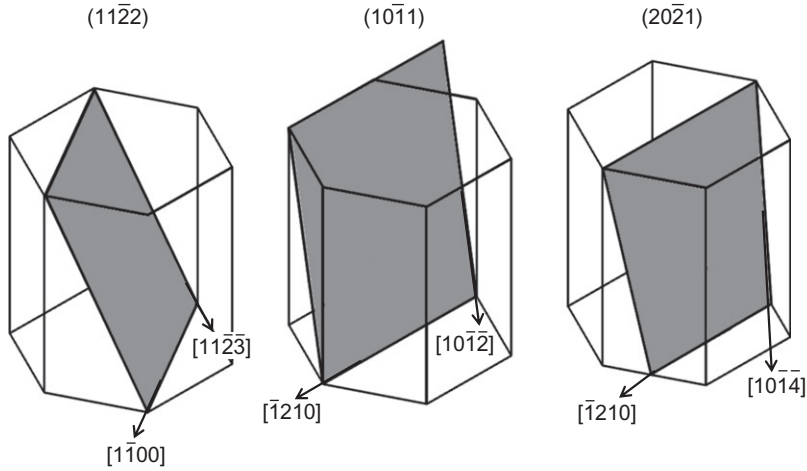

FIGURE 4.5 Various semipolar orientations of wurtzite GaN.

Fig. 4.5). The $(20\bar{2}1)$ semipolar orientation has so far shown the best performance for longer wavelength applications, owing to reduced polarization effects compared to *c*-plane, as well as other advantageous material qualities such as high compositional homogeneity in the QW (Funato *et al.*, 2010) and possibly increased indium uptake (see Section 3.2).

2.2. Band structure

The InGaN QW structure of a visible GaN LD acts as the gain medium. How easily the material achieves gain depends on several factors, some of these can be mitigated by crystal quality and design of the waveguide,

both discussed in later sections. Polarization effects, as covered in the previous section, will play an important role in gain as well, as are the energy band structure and optical properties of the material itself, covered in the following two sections.

The energy band structure of *c*-plane WZ GaN is influenced by the highly ionic nature of the material. The bottom of the conduction band is formed by 4s orbitals from the gallium atom, and the upper valence band states are formed by the 2p orbitals from the nitrogen atom (Dingle *et al.*, 1971). The upper valence band states are comprised of orbitals with x, y, and z symmetry and can separate due to the crystal-field effects of the WZ lattice and strain, depending on the crystal orientation (Morkoc *et al.*, 1998). The top heavy-hole (HH) and middle light-hole (LH) valence bands have $|X \pm iY\rangle$ symmetry, corresponding to the in-plane *a*- and *m*- directions. The lower, crystal-field split-off (SO) band has $|Z\rangle$ symmetry, corresponding to the *c*-direction (see Fig. 4.6A). Excitons involving electrons in the conduction band and holes in the HH, LH, or SO valence band are generally referred to as A, B, or C, respectively (Ghosh *et al.*, 2002).

For InGaN QWs on *c*-plane WZ GaN, the in-plane biaxial strain (as a consequence of equibiaxial stress) is isotropic and does not change the crystal symmetry in the (0001) *c*-plane, and the sequence of valence bands remains the same, although the separation of the top two valence bands and the $|Z\rangle$ valence band does change. Likewise, no in-plane

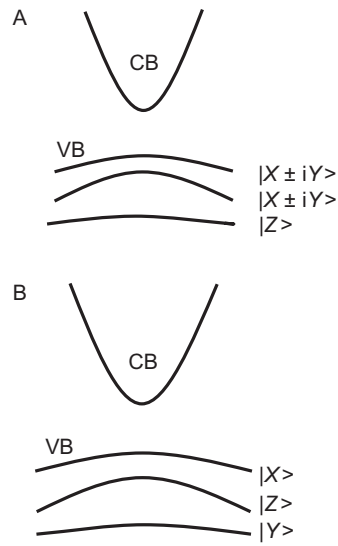

FIGURE 4.6 Schematic diagram of the energy band structure of (A) unstrained and (B) anisotropically strained wurtzite GaN, after Grahn (2009).

optical anisotropy occurs either. However, QW growth on nonpolar or semipolar orientations GaN is anisotropic in nature, arising from the polar *c*-plane laying completely or partially within the QW plane, perpendicular or inclined to growth direction, respectively. The crystal symmetry of nonpolar and semipolar planes is further reduced with anisotropic or uniaxial in-plane stress, which can modify the top valence band states and the optical anisotropy.

For nonpolar *a*- or *m*-planes, the reduced symmetry in the *x*–*y* plane divides the HH and LH band states into $|X\rangle$ and $|Y\rangle$ states, and the separation of energy between conduction band and valence band is enhanced with additional strain (Grahn, 2009). A compressive strain along the *x*-direction (*a*-direction) raises the $|X\rangle$-like valence band state and lowers $|Y\rangle$-like valence band state, lowering the energy for interband transitions between the conduction band and $|X\rangle$-like band (Masui *et al.*, 2005) – see Fig. 4.6B. Conversely, tensile strain along *x*-direction lowers the energy for interband transition between the conduction band and $|Y\rangle$-like state. As the energy band transitions are dependent on the direction and magnitude of the anisotropic strain, it is no longer possible to describe the band transitions in terms of A, B, and C excitons; instead, E_1, E_2, and E_3 are often used for the lowest, second-lowest, and third-lowest energy transitions, respectively (Ghosh *et al.*, 2002).

For compressively strained InGaN on nonpolar GaN, the lowest energy (E_1) transition is allowed for light polarized perpendicular to the *c*-axis, while the second-lowest transition (E_2) is allowed for polarizations parallel to the *c*-axis. LD waveguides involving the TE mode oriented parallel to the *c*-axis will take advantage of this anisotropy. Early theoretical results showed reduced effective mass and increased optical matrix elements for QWs on $(10\bar{1}0)$ compared to *c*-plane QWs (Niwa, 1997). Early PL measurements of QWs grown on *m*-plane GaN verified highly polarized light emission and the anisotropy of band transitions (Domen *et al.*, 1997; Gardner *et al.*, 2005). For higher indium compositions, the difference in energy transitions between E_1 and E_2 is further enhanced (Kojima *et al.*, 2008) and has been experimentally measured to be as high as 78 meV for $In_{0.15}Ga_{0.85}N$ (Schade *et al.*, 2011).

For semipolar planes, similar valence band splitting effects occur as for the nonpolar case; however, the energy separation of the top two valence band states is slightly less than for nonpolar films (Kojima *et al.*, 2008). For $(20\bar{2}1)$ InGaN QWs, polarization-dependent PL measurements verified the lowest transition energy for light polarized parallel to $[\bar{1}2\bar{1}0]$, suggesting laser stripes be oriented along the $[\bar{1}014]$ direction, parallel to the projection of the *c*-axis (Kyono *et al.*, 2010). For $(11\bar{2}2)$ InGaN QWs, polarization-dependent PL measurements verified lower energy emission for light polarized parallel to the $[1\bar{1}00]$ direction, suggesting LD stripes be oriented in the $[\bar{1}\bar{1}23]$ direction (Domen *et al.*, 1997; Kojima *et al.*, 2007).

However, additional studies found this preference may change for high-indium compositions (Ueda *et al.*, 2008), and that the lowest energy transitions for $In_xGa_{1-x}N$ QWs above (x=0.30) show the topmost valence band polarizes in the $[\bar{1}\bar{1}23]$ direction, indicating high-wavelength LDs be oriented along the $[1\bar{1}00]$ direction. Stress relaxation by misfit dislocation (MD) formation of high-indium composition InGaN QWs has been suggested as the cause of the polarization switching in semipolar heterostructures (Yan *et al.*, 2010). Relaxation mechanisms for QWs are discussed further in Section 3.2.1.

2.3. Optical polarization

The GaN crystal system is uniaxial birefringent, meaning that light polarized parallel and perpendicular to the optical axis has unequal indices of refraction, the extraordinary (n_e) and ordinary (n_o), respectively. For WZ GaN, the magnitude of this birefringence is $\Delta n = n_e - n_o = 0.011 n_o$, with the extraordinary direction pointing along the *c*-direction (Shokhovets *et al.*, 2003). If the extraordinary and ordinary directions are perpendicular to the propagation direction, then the TM and TE modes exist; however, TM modes are limited by low recombination rates so the TE mode is preferred. For edge-emitting LDs, TE emission polarized dominantly along a direction within the plane of the QW film can lead to lower threshold current density. For LDs on *c*-plane GaN, the extraordinary direction is perpendicular to the growth plane and the ordinary direction is along the growth plane, and the TE modes are polarized parallel to the growth plane (perpendicular to the *c*-axis) (Scheibenzuber *et al.*, 2009). The crystal has rotational symmetry along the QW growth plane; however, waveguides on *c*-plane LDs are typically oriented along an *m*-direction $[1\bar{1}00]$ since an *m*-face is easier to cleave for facets.

Nonpolar and semipolar layers have reduced symmetry in the QW plane, due to the anisotropic stress in the plane of the QWs, so the optical polarization of light depends on the propagation direction of the waveguide. For nonpolar $(10\bar{1}0)$ *m*-plane GaN, a waveguide orientated either parallel to *c*- or *a*-direction will show TE mode operation. However, as discussed in the previous section, the transition between the conduction band and the top valence band with the lowest transition energy (E_1) is polarized along the *a*-direction, due to the anisotropic stress in the InGaN QW, suggesting waveguide cavities be oriented along the *c*-direction (Bhattacharyya *et al.*, 2008). Okamoto *et al.* (2007a) verified that an LD waveguide oriented parallel to the *c*-axis on nonpolar GaN achieves lasing at a lower threshold (having TE mode polarization, transition involving the highest E_1 valence band, and polarized parallel to the $[11\bar{2}0]$ axis) compared to a waveguide oriented along the *a*-axis (see also Rass *et al.*, 2010b).

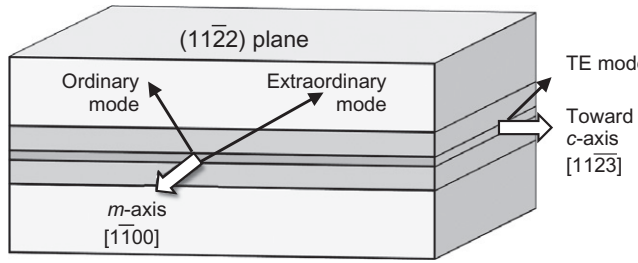

FIGURE 4.7 Schematic of possible light propagation and vector directions for various modes of $(11\bar{2}2)$ LD, after Sizov *et al.* (2011).

For semipolar LDs, light polarized at an inclined angle to the *c*-direction will be influenced by both ordinary and extraordinary components, which can cause the light to travel at different speeds and result in a rotation of the electric field vector. Semipolar waveguides oriented along the projection of the *c*-axis will have TE (transverse electric) and TM (transverse magnetic) polarization; however, waveguides oriented at inclined angles to the *c*-direction will not have TE and TM polarized modes, but rather ordinary and extraordinary like modes, which may compete with the transverse waveguiding (described later in Section 4) (see also Huang *et al.*, 2010b; Scheibenzuber *et al.*, 2009). See Fig. 4.7 for a schematic of mode orientation for semipolar $(11\bar{2}2)$.

For LDs on $(11\bar{2}2)$, TE mode gain should be higher for waveguides oriented along the $[\bar{1}\bar{1}23]$ direction as opposed to the $[1\bar{1}00]$ direction due to birefringence effects, which coincides with the waveguide preference for upper valence band transition. Several groups have verified this stripe orientation by demonstrating lower threshold power densities for optically stimulated waveguides on $(11\bar{2}2)$ (see Kojima *et al.*, 2007; Rass *et al.*, 2010b; Tyagi *et al.*, 2008). For LDs on semipolar $(20\bar{2}1)$, the gain should be higher for waveguides oriented along the $[\bar{1}014]$ direction, also coinciding with the stripe preference of the upper valence band transitions. Sumitomo Electric verified lower lasing thresholds in this direction compared to the $[12\bar{1}0]$ direction (Kyono *et al.*, 2010). However, as is the case for $(11\bar{2}2)$, cleaved facets may not be available for waveguides oriented in this direction, in which case the facets must be formed by etching (see Section 4.4).

2.4. Gain

Calculation of gain for alternative planes of GaN has to take into account several material properties with key differences between the polar, nonpolar, and semipolar planes. Electron and hole wave function envelopes effecting the recombination matrix elements are highly impacted by the

magnitude of polarization discontinuities between InGaN and GaN, as explained in Section 2.1. The electronic spectra based on the valence band states discussed in Section 2.2 also play an important role as do the optical anisotropy and choice of waveguide orientation. More details on gain calculations can be found in Scheibenzuber *et al.* (2009). Their results comparing material gain for TE modes of polar, nonpolar, and semipolar are summarized in Fig. 4.8, which shows calculated gain at various sheet carrier densities for TE modes. Again, for nonpolar or semipolar planes, the TE modes exist with the waveguides oriented parallel to the *c*-axis or a direction parallel to the projection of the *c*-axis, respectively.

Positive gain is possible for extraordinary and ordinary mode waveguides, such as for semipolar planes oriented perpendicular to the *c*-direction direction. Although the maximum gain is reduced than for TE modes, waveguides oriented along the non-*c*-direction may reach transparency at a lower excitation powers than the preferred stripe orientation. Sizov *et al.* (2011) verified this effect with optically pumped lasing of pure green $(11\bar{2}2)$ LDs with stripes along the *m*-direction, using a low-loss waveguide with cleaved *m*-facets.

2.5. Summary

The inherent asymmetry of GaN puts several limitations on this material system for LD applications, particularly for the *c*-plane crystal orientation. The strong spontaneous electrical polarization and strain-induced polarization due to high lattice mismatch with ternary alloys reduce radiative efficiencies and blue-shifts wavelengths with current density. The QCSE increases for higher indium composition InGaN alloys, challenging high-wavelength LD applications. For nonpolar and semipolar planes, the crystallographic asymmetry causes some anisotropy in the growth plane, leading to anisotropy in the optical characteristics and gain and a preferred waveguide direction. Provided they are oriented along the preferred crystal direction, nonpolar and semipolar orientations show high material gain values for TE polarized modes, certainly a major advantage over *c*-plane GaN for LDs.

The reduced polarization and high material gain would leave us to expect low-threshold current densities for nonpolar and semipolar planes. However, the same effects that give the nonbasal planes high radiative efficiency will also increase spontaneous emission, leaving them susceptible to Auger recombination and decreased charge-carrier lifetimes. There are also other growth-related issues and LD design issues related to nonpolar and semipolar growth that makes the story a little more complicated, discussed next.

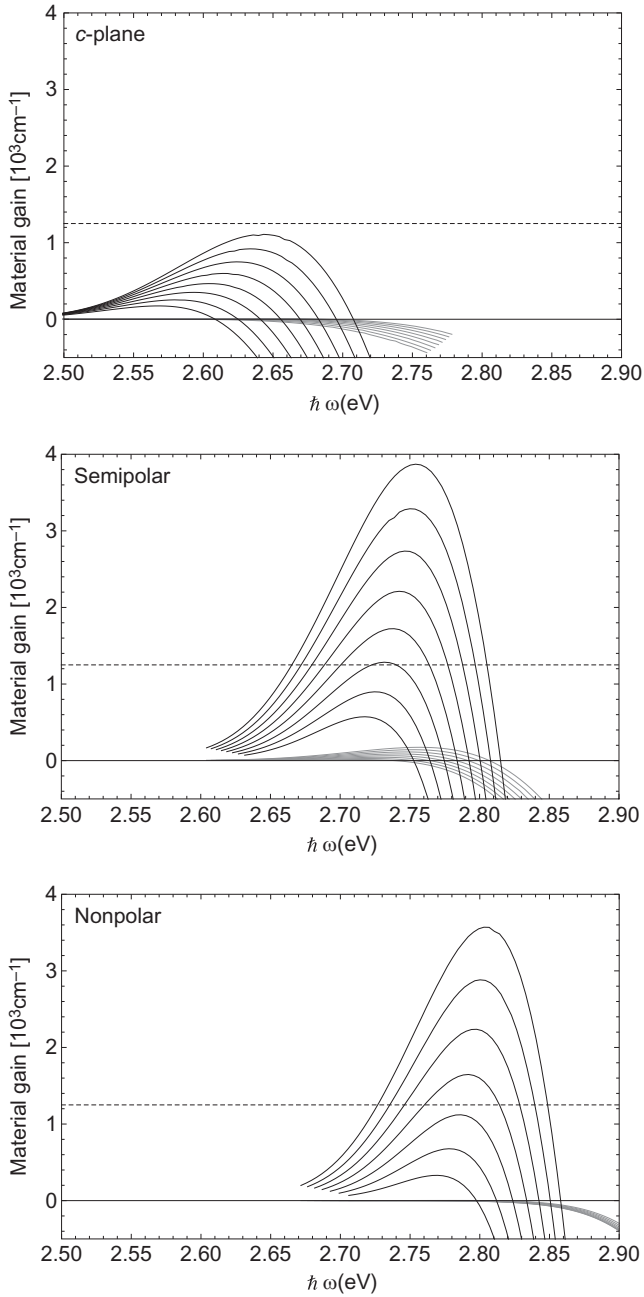

FIGURE 4.8 Calculated modal gain for TE modes (black) and TM modes (gray) for polar, semipolar, and nonpolar GaN LDs oriented parallel to the *c*-axis or projection of the *c*-axis. The dashed line represents estimated threshold gain. Results are for sheet carrier densities are from bottom to top 5×10^{12}–$8.5\times10^{12}\,\mathrm{cm}^{-2}$ *c*-plane, 4×10^{12}–$7.5\times10^{12}\,\mathrm{cm}^{-2}$ semipolar, and 3×10^{12}–$6\times10^{12}\,\mathrm{cm}^{-2}$ nonpolar in steps of $0.5\times10^{12}\,\mathrm{cm}^{-2}$. Data from Scheibenzuber *et al.* (2009), used by permission. Copyright (2009) by the American Physical Society.

3. GROWTH ISSUES

Metal organic chemical vapor deposition (MOCVD) growth of group-III nitrides commonly uses trimethyl or triethyl compounds of aluminum, gallium, and indium as group-III precursors, and ammonia as group-V precursor. The growth of these layers requires special precautions to avoid pre-reactions of organometallic gallium and ammonia to ensure the sources reaching the heated substrate. Pre-reactions can be controlled by optimization of the growth conditions such as high flow rates or reduced pressure to shorten the residence time of the precursor molecules in the heated zone of the growth chamber (DenBaars and Keller, 1997). Pre-reactions, which can cause reduction in growth rates and can adversely affect material quality, can also be prevented with a careful reactor design, such as a two-flow MOCVD technique developed by Nakamura *et al.* (2000).

3.1. Substrates

One of the primary obstacles in the development of *c*-plane GaN devices was the lack of native GaN substrates. Early GaN growths explored a variety of nonnative substrates such as spinel ($MgAl_2O_4$) and SiC; however, sapphire remains the most commonly used. With a 13% lattice mismatch, GaN grown on sapphire substrates can suffer from a high density of defects and threading dislocations (TDs) which limits device performance through the formation of nonradiative recombination centers. The first GaN LD was demonstrated on GaN buffers grown on sapphire, despite a large TD density of 10^{10}cm^{-2} (Nakamura *et al.*, 2000). Since then, the implementation of thick buffer template layers, epitaxial lateral overgrowth (ELOG) techniques, or other patterning techniques can help reduce TD densities several orders of magnitude and can significantly improve GaN LD performance and lifetimes (Takeya *et al.*, 2005). Bulk *c*-plane GaN substrates with TD densities in the 10^1–10^4cm^{-2} range may be soon available by high nitrogen pressure or ammonothermal methods (see Dwiliński *et al.*, 2009; Grzegory and Porowski, 2000; Kucharski *et al.*, 2009).

Substrate availability played a large role in development of devices on nonpolar and semipolar planes of GaN as well. The first planar nonpolar GaN growths were demonstrated on (100)-oriented γ-$LiAlO_2$ (Waltereit *et al.*, 2000) and *r*-plane $(10\bar{1}2)$ sapphire (Craven *et al.*, 2002), and the first nonpolar GaN-based LEDs were demonstrated on *m*-plane SiC substrates (Gardner *et al.*, 2005). Early semipolar GaN-based LEDs planes were achieved on foreign substrates such as *m*-plane sapphire (Sharma *et al.*, 2005), (100), and (110) oriented spinel (Chakraborty *et al.*, 2005a). Another method used is overgrowth of patterned stripes oriented along the *m*-plane $\{10\bar{1}0\}$ of *c*-plane GaN substrates to form stable facets and strong luminescence in the $(11\bar{2}2)$ semipolar plane (Nishizuka *et al.*, 2004).

Like *c*-plane grown on foreign substrates, nonpolar and semipolar films on foreign substrates suffer from high densities of TDs (in excess of 10^{10}cm^{-2}) and basal-plane stacking fault (BPSF) densities from 10^5–10^6 cm^{-1} which can severely degrade device performance (Craven *et al.*, 2002). The years that followed saw significant developments on growth of native nonpolar and semipolar substrates (Chakraborty *et al.*, 2005b; Haskell *et al.*, 2003, 2005). In addition to reduced TD densities, bulk freestanding GaN substrates are beneficial as they eliminate the mismatch of thermal expansion coefficient, facilitate formation of cleaved facets and allow backside contacts. GaN substrates are also preferred from a waveguiding perspective because the index-mismatch between nonnative substrates and GaN template growth can form a parasitic waveguide and leaky optical modes in the nonnative substrate.

In 2006, low-defect density bulk nonpolar *m*-plane (Fujito *et al.*, 2009) and semipolar $(11\bar{2}2)$ substrates (Funato *et al.*, 2006) were made available by Mitsubishi Chemical Corporation and Furukawa Co., Ltd., respectively. These substrates are grown very thick in the basal *c*-plane direction by HVPE, then sliced at different angles and polished to form an epi-ready surface. Subsequent results on violet *m*-plane LEDs (Kim *et al.*, 2007b) and $(11\bar{2}2)$ LEDs in the blue, green, and amber wavelengths (Funato *et al.*, 2006) showed improved performance over previously published nonpolar and semipolar results, attributed to reduction in defects. The first demonstrations of electrically injected lasers on freestanding *m*-plane substrates, $(10\bar{1}1)$ substrates (Tyagi *et al.*, 2007), and stimulated emission on $(11\bar{2}2)$ substrates (Kojima *et al.*, 2007; Tyagi *et al.*, 2008) were soon to follow. It is no doubt that the availability of low-defect density nonpolar and semipolar substrates was the technological breakthrough needed to finally allow nonbasal LDs to compete with already maturing *c*-plane LD technologies. In the years that followed, UCSB explored intentionally miscut *m*-plane substrates to prevent formation of pyramidal hillocks formed by pinned steps around TDs (Farrell *et al.*, 2010a; Hirai *et al.*, 2007). Morphologically, smooth template growths that resulted on *m*-plane GaN with 1° miscut toward $[000\bar{1}]$ showed improved device characteristics including uniform PL emission and lower threshold current densities compared to on-axis growths (Lin *et al.*, 2009b). In late 2010, Sumitomo announced development of 2-in. bulk nonpolar and semipolar substrates, which will enable improved manufacturability and yield for nonbasal LD devices (Sumitomo, 2010).

3.2. InGaN growth

For indium to incorporate onto GaN requires reduced growth temperatures, generally hundreds of degrees less than typical GaN template growth. These low-growth temperatures allow the indium-containing

precursor tri-methyl-indium to desorb onto the growth surface and incorporate into the film. For most MOCVD growth of InGaN, temperature is used to fine-tune the indium composition and thus emission wavelength of the layers. For devices operating at wavelengths that require high-indium content InGaN QWs in the active region, the QW growth is challenged by growth instabilities at lower growth temperatures. Formation of indium droplets and the generation of defects in In-rich InGaN due to growth errors or strain relaxation can all severely degrade device performance. Some methods for mitigating these effects include growing thinner wells, modifying barrier compositions, and reducing background Mg doping (Miyoshi *et al.*, 2010; Queren *et al.*, 2009a,b; Strauss *et al.*, 2008a).

Another factor in growing high-indium content QWs is the indium composition efficiency of the substrate, or indium uptake, which can depend highly on the orientation of crystal plane. Crystal planes with low uptake levels require lower growth temperatures at otherwise similar growth conditions to realize the same indium composition as planes with high uptake levels. There are some indications that semipolar planes show the highest indium incorporation efficiencies compared to other planes – possibly because these inclined planes expose binding sites for Ga and In atoms that more easily incorporate In atoms than sites available on the (0001) and $(10\bar{1}0)$ surfaces (Northrup and Neugebauer, 1999). Coloaded growths of $(1\bar{1}01)$ side facets showed 50% higher indium incorporation compared to *c*-plane (Wunderer *et al.*, 2008), and in another study, $(11\bar{2}2)$ plane shows up to 30% higher indium incorporation compared to *c*-plane (De Mierry *et al.*, 2009). However, these results contrast with other coloaded growth studies and seem to be highly reactor dependent. Early demonstration of yellow LEDs on $(11\bar{2}2)$ may indicate this plane does have higher indium uptake compared to other planes (Sato *et al.*, 2008).

While further studies may be necessary, nonpolar *m*-plane appears to show the lowest indium uptake compared to *c*-plane, most likely due to the low chemical reactivity and low cohesive energy of the In-N bond on charge neutral *m*-plane (Chichibu *et al.*, 2008; Yamada *et al.*, 2008b). Low indium uptake may make *m*-plane more prone to growth errors due to the low-growth temperature required for increased indium compositions. Transmission electron microscopy studies of high-indium composition (x=0.26) $In_xGa_{1-x}N$ QWs on *m*-plane GaN verified formation of I_1 BPSFs with Burgers vectors $\boldsymbol{b} = 1/6\langle 2\bar{2}03\rangle$ (Wu *et al.*, 2010). This type of fault can be formed by the removal of a basal plane followed by subsequent relaxation and changes the stacking sequence to *ABABABCBCBC*. The SFs are bound by sessile Frank–Shockley partial dislocations. For high-indium composition QWs on *m*-plane, the density of dislocations (mostly partial dislocations that terminate the stacking faults) can increase by several orders of magnitude over the inherent TD density from the

substrate. The authors (Wu *et al.*, 2010) note that this type of dislocation formation is generally associated with a type of growth error, not a slip mechanism related to strain relaxation. Strain relaxation of InGaN films on *m*-plane as well as semipolar planes has been observed, described in the following section.

3.2.1. InGaN strain limits and relaxation

InN and GaN have a lattice mismatch of 11% and InGaN typically grows pseudomorphically on GaN templates. Stresses due to the lattice mismatch become more severe at long wavelengths. For blue-emitting QWs of $In_{0.18}Ga_{0.82}N$, the mismatch is 1.8%; for green-emitting QWs of $In_{0.3}Ga_{0.7}N$, the mismatch is 3%. Eventually, any InGaN layer will reach a thickness at which misfit stress relaxation is favored either by 3D growth, followed by dislocation-related relaxation, or directly by MD formation as defined as the Matthews–Blakeslee critical thickness (Matthews and Blakeslee, 1974). Avoiding this critical thickness becomes another important consideration with LD waveguide design, especially for high-indium composition QWs or relatively thick (over 50nm) InGaN waveguiding layers, described later in Section 4.2.

Relaxation of InGaN can take many forms, but the easiest form is via an available slip system for MD formation via glide on the (0001) *c*-plane. However, only slip systems oblique to the basal plane that can resolve misfit stress and contribute to plastic relaxation in this manner. For polar *c*-plane, the main slip system lays parallel to the interface with GaN, leading to zero-resolved shear stress along the growth direction. Relaxation of InGaN on *c*-plane GaN may occur due to local shear stresses around three-dimensional features formed around defects, such as V-defects (Srinivasan *et al.*, 2003).

For nonpolar $(11\bar{2}0)$ *a*-plane or $(1\bar{1}00)$ *m*-plane, the basal plane is orthogonal to the growth plane, so slip along the [0001] direction should not occur for thick InGaN due to the absence of shear stresses along this preferred basal-oriented slip plane. Stacking fault generation of high-indium composition QWs on *m*-plane GaN, as discussed in the previous section, promotes the emergence of dislocations with a basal plane component that, as early studies indicated, may relieve compressive stresses related to InGaN/GaN lattice mismatch (Fischer *et al.*, 2009; Wu *et al.*, 2010). Recent studies of thick InGaN films on *m*-plane GaN by Yoshida (2011) verified coherent growth along the [0001] direction and the emergence of macroscopic tilt along two $[11\bar{2}0]$ directions, indicating slip corresponding to the $\{10\bar{1}0\}$ prism plane.

For semipolar planes, the basal plane is inclined to the growth plane, so the easy basal-plane slip system is available for film relaxation. Shear stresses tend to form one-dimensional arrays of MDs along a single direction, where the initial stage of MD formation proceeds by the bending and glide of preexisting TDs on the (0001) slip plane (Hsu *et al.*, 2011).

Because of the oblique angle, the MD Burgers vector has two components. The in-plane component of the MD Burgers vector $b||$ is responsible for diminishing the stress caused by lattice mismatch, the out-of-plane component $b\perp$ will cause lattice tilt of the epi-layer (Romanov *et al.*, 2011). The composition and strain state for thin films can be quantified by a single symmetric on-axis reciprocal space map, or four symmetric on-axis rocking curve X-ray measurements, due to the initial one-dimensional nature of the strain relaxation (Young *et al.*, 2011).

For $(11\bar{2}2)$ substrates, the formation of MDs can be characterized with an in-plane direction $[\bar{1}100]$, originating from preexisting TD of $\mathbf{a}_3$-type with Burgers vectors $\boldsymbol{b} = a/3[\bar{1}120]$. This type of dislocation is pure-edge type with large in-plane component for strain relaxation compared to mixed edge-screw $\mathbf{a}_1$ and $\mathbf{a}_2$ types (Hsu *et al.*, 2011; Tyagi *et al.*, 2009; Young *et al.*, 2010b). Tilt was also observed with angles up to 0.66° parallel to $[\bar{1}123]$ (and minimal tilt parallel to $[\bar{1}100]$) for single green-emitting QWs grown on low InGaN composition underlayers, simulating waveguiding structure discussed later in Section 4.2.

On semipolar (20-21) GaN, InGaN films can experience similar relaxation mechanisms for MD generation as in (11-22), with MDs forming along the a-direction [11-20]. However, due to the higher inclination angle with respect to the (0001) plane (~75° vs. 58°), the resolved shear stresses on $(20\bar{2}1)$ are lower for otherwise the same InGaN–GaN lattice mismatch as on $(11\bar{2}2)$, leading to higher critical thickness (37.7 nm vs. 29 nm for $In_{0.07}Ga_{0.93}N$) (Romanov *et al.*, 2011).

Since MD formation is less likely on $(20\bar{2}1)$ for the same indium composition compared to other semipolar planes, it may explain why this particular plane has had more success for long-wavelength LDs applications (Young *et al.*, 2010a). For InGaN QWs on $(20\bar{2}1)$ with very high-indium compositions, however, defects in the QWs will eventually form and can be observed as a formation of dark triangles viewable under fluorescence (Lin *et al.*, 2010). These dark areas seem to be mitigated by lattice-matched quaternary AlInGaN underlayers, which may reduce strain in the QW region (Enya *et al.*, 2009). AlGaN barriers between the QWs also showed improved emission uniformity and LED efficiency (Lin *et al.*, 2010), probably due to strain mitigation.

3.3. AlGaN growth and relaxation

There are several growth challenges involved with the growth of high-quality AlGaN, especially thick layers of high aluminum composition used for laser cladding layers (see Section 4.2). During AlGaN growth by MOCVD, parasitic pre-reactions can cause formation of nonvolatile adducts between the aluminum precursor trimethylaluminum (TMA) and ammonia (Tokunaga *et al.*, 2008). The pre-reactions can deplete the

amount of TMA in the gas phase and consequently limit the Al incorporation in the epitaxial AlGaN film. Further, the reaction can cause particulates to deposit on the reactor surfaces or incorporate into the film, which can reduce reactor stability, device lifetime, and yield (Feezell *et al.*, 2007). Mg-doped AlGaN has higher electrical resistivity and poorer structural quality compared to Mg-doped GaN. AlGaN layers are also more also sensitive to oxygen impurity incorporation, which act as donors and further reduce p-doping efficiency (Jang *et al.*, 2004). For these reasons, avoiding AlGaN-cladding layers for LD waveguide designs may have advantages, described later in Section 4.2.

AlN has a 2.4% lattice mismatch to GaN, and tensile-strained AlGaN layers on GaN will eventually relax by formation of cracks and possibly MDs. Like InGaN, the thickness limit and nature of relaxation is highly dependent on the crystal orientation of the GaN substrate and can restrict the design space of LD waveguides on these planes. The critical thickness for dislocation formation is generally smaller than for cracking for most heteroepitaxial film growth (Matthews and Blakeslee, 1974); however, dislocations of AlGaN films require availability of the basal plane slip system to propagate. For polar (0001)-oriented GaN-based layers, the slip systems are not readily available due to zero-resolved shear stresses, no interfacial dislocations with an in-plane edge component, and large kinetic barriers to glide (Hearne *et al.*, 2000). Instead, misfit stress in AlGaN on *c*-plane GaN films initially relaxes by cracking, followed by MDs forming in pyramidal or prismatic slip systems originating at the crack sites.

Nonpolar *m*-plane GaN also has no resolved shear stress on the basal plane, so AlGaN films also relax by cracking, generally along the *c*-plane (Okamoto *et al.*, 2008), and generally are not accompanied by MDs. The strain and ease of crack formation along the *c*-plane in nonpolar *m*-plane devices may promote the formation of cleaved facets on the *c*-plane (see Section 4.4), reinforcing the preference for *c*-plane-oriented ridges on nonpolar *m*-plane as discussed in Sections 2.2 and 2.3. In fact, the addition of AlGaN layers in otherwise AlGaN-free structures has shown to improve cleaved facet yield for *m*-plane LDs (Hardy *et al.*, 2011).

For AlGaN on semipolar GaN, stress relaxation via MD formation by slip is viable due to the presence of resolved shear stress on the basal (0001) plane. Glide is more likely to occur than cracking, centered at preexisting TDs. The lattice misfit parameter is approximately equal in sign but reverse in magnitude as with InGaN films. Please refer to Romanov *et al.* (2011) for a summary of critical thickness of AlGaN for semipolar planes inclined at arbitrary angles from the *c*-plane.

3.4. Summary

From Section 2, it would appear that nonpolar *m*-plane has the best overall material properties for long-wavelength LD applications due to zero polarization discontinuities and highest predicted material gain.

Indeed, very competitive LD results have been demonstrated in violet (Farrell *et al.*, 2010b) and blue wavelengths (Okamoto *et al.*, 2008) in terms of threshold current density and slope efficiency. However, due to the low indium uptake and propensity for growth errors at low-growth temperatures, green LDs on nonpolar *m*-plane have yet to be demonstrated. LEDs on nonpolar *m*-plane show a marked drop-off in output power for wavelengths above 500nm, likely due to SF generation within the QW (Lin *et al.*, 2010) due to growth errors at low-growth temperatures or relaxation at high-indium compositions (Yoshida *et al.*, 2011). To date, the highest reporting lasing wavelength on *m*-plane is 499.8nm (Okamoto *et al.*, 2009).

Semipolar films may be somewhat limited by some of the same polarization effects as *c*-plane, and InGaN and AlGaN films on semipolar substrates have a propensity for MD formation due to strain relaxation. Still, for green applications, semipolar $(20\bar{2}1)$ may still offer the best overall characteristics. Only 15° from the nonpolar *m*-plane, $(20\bar{2}1)$ sees significantly reduced QCSE compared to *c*-plane, appears to have higher indium uptake levels compared to nonpolar *m*-plane (allowing higher InGaN QW growth temperatures), and improves stress relaxation limits compared to semipolar $(11\bar{2}2)$. The highest wavelength LDs reported at the time of writing are on $(20\bar{2}1)$ (Ueno *et al.*, 2011), an achievement reached only 2 years after the first LD ever reported on that crystal plane. UCSB recently reported low droop and high-output power LEDs grown on $(20\bar{2}\bar{1})$ (Zhao *et al.*, 2011). This plane is oriented at an equal but opposite angle from the *c*-plane as $(20\bar{2}1)$ and may eventually offer improved performance on LD applications as well.

4. LASER DIODE DESIGN ON ALTERNATIVE GaN PLANES

As discussed in previous sections, nonpolar and semipolar crystal orientations of GaN have advantages over standard *c*-plane GaN for visible LD application in terms of higher emission efficiency and higher material gain. Modal gain in an LD has multiple components: the intrinsic material gain that depends on transition efficiencies, band structure, and injection level, and the optical mode confinement. The transparency current density for GaN LDs is 10 times that in GaAs (Uchida *et al.*, 2003), so GaN LDs require much higher carrier concentrations to reach the necessary population inversion to reach lasing threshold. Therefore, reducing losses and maximizing mode confinement are very important for increasing the WPE for GaN LDs. Toward this goal, the waveguide cavity must minimize potential losses by providing adequate electrical confinement, carrier confinement, and optical confinement. Figure 4.9 shows a schematic of a typical ridge waveguide used for edge-emitting GaN-based LDs.

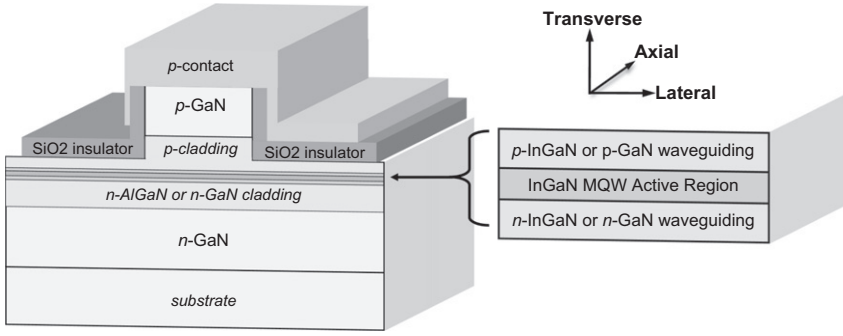

FIGURE 4.9 Three-dimensional schematic of a typical GaN ridge waveguide employing an SiO_2 oxide sidewall insulator.

This section outlines some considerations for GaN LD waveguide design and how it may be influenced by crystal orientation. The differing material properties of basal and nonbasal crystal planes of GaN puts different constraints on the transverse waveguide design, active region, waveguiding layers, and cladding layers, all of which play a large part in device performance and overall manufacturability of LDs.

4.1. Absorption loss

Direct measurements of gain spectra of GaN lasers report relatively high internal losses (15–30 cm^{-1}) (Schwarz *et al.*, 2007). Direct free-carrier absorption should be insignificant in GaN, due to a lack of hole states available in a relevant energy range and dipole-forbidden transitions of free electrons to the second conduction band (at 2.5 eV above the band minimum) (Kioupakis *et al.*, 2010a). However, free-carrier absorption via indirect phonon-assisted processes likely contributes a significant fraction of the total optical loss. Early on in GaN LD development, absorption within the Mg- and Si-doped regions of the waveguiding and cladding layers were determined be a dominant loss mechanism, with Mg-doped GaN providing the largest contribution, up to 100 cm^{-1} (Kuramoto *et al.*, 2002). First-principle calculations from Kioupakis *et al.* (2010b) has elucidated the impact of phonon-assisted absorption of holes in the p-doped waveguiding and cladding layers as dominant loss mechanism in GaN LDs. Influenced by large acceptor activation energy (0.2 eV for Mg) (Van de Walle and Neugebauer, 2004), p-type GaN contains a high fraction of nonionized acceptors, requiring high doping concentrations ($\sim 10^{19}$ cm^{-3}) to achieve adequate free-hole densities. Combining the high density of bound carriers of p-doped GaN and high-mode overlap with p-doped waveguiding and cladding layers leads to a high

contribution to total loss, approximately 75% of the total optical loss. Si-doped layers provide a much smaller contribution due to relatively lower dopant concentrations ($\sim 10^{18}$ cm^{-3}). Other indirect free-carrier absorption effects may contribute a small amount toward total loss and include scattering at charged defects and InGaN alloy fluctuations. Alloy-assisted absorption in InGaN QWs actually increases with indium composition, so will have a larger influence on loss for higher-wavelength LDs. However, as the optical mode overlap (Γ) with the QWs is low (typical values are 3–5%), their overall contribution of loss is small.

Reducing loss in the p-doped layers can be achieved several ways, including reducing doping of the p-doped areas closest to the active region where optical mode overlap is highest, approximately 16–23% in the waveguiding and cladding layers, respectively (Kioupakis *et al.*, 2010b). Another method employs an asymmetric waveguide structure that shifts the optical mode overlap toward the less-lossy *n*-side (see Huang *et al.*, 2010a; Kneissl *et al.*, 1999; Kuramoto *et al.*, 2002). Using a dopant with lower activation energy such as Be has also been suggested to reduce the acceptor concentration necessary for suitable p-GaN conductivity (Neugebauer and Van De Walle, 1999).

4.2. Transverse waveguiding

For optical confinement in the transverse direction (parallel to the grown direction), the waveguide must provide adequate index contrast for mode confinement, provided the layers are unrelaxed with a low-defect density, and able to maximize carrier injection and recombination. For low-threshold LDs, high optical confinement in the QW region is necessary to maximize gain. Poorly confined modes are subject to losses, either as leaky modes into a nonnative substrate (as explained in Section 3.1), high-absorption losses in the Mg-doped side, or optical interactions with the contact metal.

High-mode confinement in the transverse direction can be achieved by increasing the refractive index within or near the active region, by increasing number or thickness of QWs, or using InGaN waveguiding layers above and below the QWs. High-mode confinement may also be achieved by increasing the index contrast with lower index outer-cladding layers, such as bulk AlGaN or AlGaN/GaN superlattices. A typical waveguide design can employ (In)GaN waveguiding and (Al)GaN cladding layers and is shown in Fig. 4.10A.

The InGaN QW active region must be designed to maximize carrier injection and optical confinement. As previously discussed in Section 2.1, additional strain caused by the heteroepitaxy of lattice-mismatched InGaN on GaN substrates can be detrimental to QWs grown on the polar orientation due to the QCSE, so QWs on *c*-plane LDs are limited

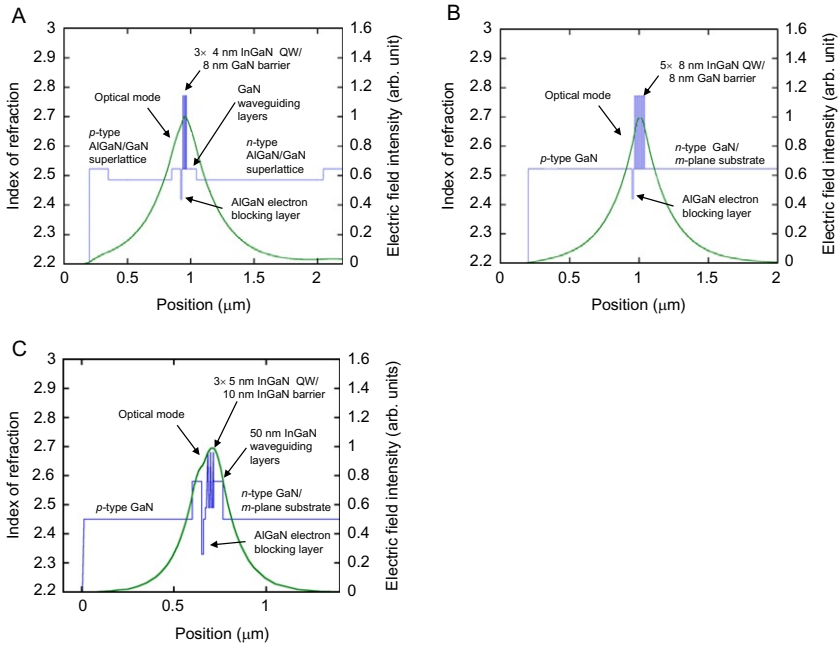

FIGURE 4.10 Comparison of refractive index of the transverse waveguide and calculated and mode overlap of the primary optical mode for (A) typical violet *c*-plane waveguide structure and (B) violet ACF *m*-plane LD structure, after Farrell (2010), and (C) blue ACF with InGaN SCH waveguiding layers waveguide, after Kelchner *et al.* (2009).

in thickness, generally less 3nm. Nonpolar and semipolar GaN are already advantaged because of their intrinsically high radiative efficiencies and high material gain. Early demonstration of nonpolar GaN LEDs in the violet region showed that InGaN QWs do not suffer from a loss in efficiency with increased thickness (as in *c*-plane), even up to 18nm, due to the lack of polarization-induced fields (as mentioned in Section 2.1) (Kim *et al.*, 2007a). This was another great advantage of nonpolar GaN for LD applications, as increasing the QW width is a simple means to increase both optical mode confinement and electrical confinement.

Nonpolar *m*-plane GaN LDs with thick QWs were the basis of a simplified AlGaN-cladding-free (ACF) LD design developed by UCSB that uses only wide QWs and GaN waveguiding and cladding layers (Feezell *et al.*, 2007) and (Farrell *et al.*, 2007). The large active region volume provided by the thick wells sufficiently confines the optical mode ($\Gamma \sim 16\%$), as shown in Fig. 4.10B (Farrell, 2010). The simplified LD structure is very similar to an LED design, requiring lower growth time in the reactor, leading to higher throughput of LD growths. In addition, by using bulk native GaN substrates, leaky modes escaping into the substrate

are absent. Further, removing AlGaN cladding has significant practical implications such as avoiding parasitic effects of AlGaN precursor reactions during the MOCVD growth, and increased resistivity of AlGaN layers, as explained in Section 3.3.

However, it is important to note that there is some design trade-off with an ACF design, as wide QWs may also reduce the subband separation and carrier distribution between them, which can ultimately reduce gain (Kisin *et al.*, 2009). In addition, increased QW widths are difficult for longer wavelengths on all the crystal orientations of GaN. High-indium compositions are difficult for basal plane due to increased QCSE, difficult for nonpolar *m*-plane due to reduced indium update and a propensity for SF formation, and semipolar planes due to stress relaxation limits, as discussed in Section 3.2. Further, the index contrast between InGaN and GaN and AlGaN all reduce with wavelength due to dispersion effects, so for longer wavelength applications additional waveguiding is key (Lermer *et al.*, 2010).

Thick (50nm) InGaN layers ranging from 5% to 10% in composition can be used as waveguiding layers close to the active region to help confine the optical mode (Okamoto *et al.*, 2007b). This design is also referred to as a separate confinement heterostructure (SCH) design and is common among most semiconductor LD designs. In the blue region, UCSB's ACF LD design was modified with the addition of InGaN SCH waveguiding layers above and below the active region, shown in Fig. 4.10C, which increases mode confinement from ~2.4% to 4.9% for a 3×5nm MQW active region in the blue spectrum (Kelchner *et al.*, 2009). This design was used to demonstrate pulsed and CW operation (Kelchner *et al.*, 2010) for true-blue *m*-plane LDs. A similar ACF with InGaN SCH waveguide was also demonstrated in pulsed-lasing mode for blue-green *m*-plane LDs (Lin *et al.*, 2009b) as well as blue-green semipolar LDs (Hsu *et al.*, 2010; Tyagi *et al.*, 2010). Employing a similar LD design in the violet region maximized optical mode confinement ($\Gamma \sim 8.7\%$) compared to the violet ACF design of Fig. 4.10B and reduced lasing thresholds to 1.54kA/cm^2, competitive with state-of-the-art *c*-plane (Farrell *et al.*, 2010b).

Most commercial LD designs still employ AlGaN-cladding layers and optimizations of aluminum composition, thickness, and placement relative to the active region have been extensively studied to maximize confinement factor and reduce optical losses or leaky modes for a variety of wavelengths (Huang *et al.*, 2010a; Ryu *et al.*, 2009; Zhang *et al.*, 2009). To avoid the high loss of Mg-doped upper p-AlGaN layers, asymmetric waveguide design has been demonstrated using n-AlGaN and p-GaN cladding (Lin *et al.*, 2009c). Designs without p-AlGaN show improved electrical characteristics, due to higher hole concentration and hole mobility in p-GaN layers (Dorsaz *et al.*, 2010). While Si-doped n-AlGaN-cladding layers generally contribute less to total loss, they must still be of sound

structural quality and surface morphology for subsequent active region growth. It is important to stay below the stress relaxation limit for these layers to prevent detrimental effects such as dislocation generation due to strain relaxation by cracking on-polar and nonpolar planes, or by slip on semipolar planes, as discussed in Sections 3.3. To prevent strain relaxation, AlGaN/GaN superlattices may be used instead of thick bulk AlGaN layers. Sumitomo reported use of quaternary InAlGaN-cladding layers to reduced lattice mismatch and yet still provide enough refractive index contrast for optical confinement needed to demonstrate high-wavelength $(20\bar{2}1)$ LDs (Ueno *et al.*, 2011).

4.3. Lateral waveguiding

For carrier confinement and optical confinement in the lateral direction, laser stripes are formed with processing techniques postgrowth. The most popular designs in GaN LDs are simple broad-area and ridge waveguides. Broad-area or gain-guided waveguides were used in the earliest GaN LD demonstrations. This design employs an insulating oxide layer with an aperture at the top p-GaN surface to provide some current confinement. Although easy to fabricate, the injected carriers are free to diffuse laterally underneath the stripe and the optical mode can be poorly confined – both can be significant sources of loss. The ridge waveguide shown in Fig. 4.9 relies on index guiding from dry-etching stripes into the p-GaN and passivating the sidewalls with an insulating oxide such as SiO_2. This design combines current and photon confinement, the latter due to the effective index of refraction being reduced for areas outside of the ridge.

The ridge width and depth can affect the lateral mode confinement and the number of lasing modes. Narrow ridge widths allow single-mode operation and can support reduced spot sizes needed for flying spot laser projection. However, the optimal ridge width competes with current spreading and increase losses due to decreased lateral mode confinement (Müller *et al.*, 2010). The maximum ridge width (w) for single-mode operation depends on wavelength, index contrast of the waveguide elements, and effective refractive index (Strauss *et al.*, 2008b). Typical ridge widths for single-mode operation of GaN LDs are around 1–2 μm.

The height of the ridge must also be carefully designed for proper waveguiding of the preferred lasing modes. Most ridge designs employ an etch into the p-GaN, stopping above the active region. Due to the large difference in etch rate for GaN and AlGaN, AlGaN layers may be used as etch-stop layers to control the depth of the ridge etch, as demonstrated by Farrell *et al.* (2011). For reduced threshold current density, increasing the etch depth of the ridge waveguide through the QW region may reduce lateral carrier losses (Kelchner, 2012). However, there is some tradeoff

with this technique as expected etching too close to the active region can negatively affect the number of modes and effect far-field beam quality and etching through the active region can increase nonradiative recombination or photon scattering at the ridge sidewall, increasing losses (Schwarz *et al.*, 2005). High-power LD applications generally employ wide ridges to allow multiple lateral modes, which helps broaden the optical intensity at the facets to avoid catastrophic optical damage (COD).

4.4. Laser facets

For edge-emitting in-plane LDs, mirrored facets that provide optical feedback along the axial direction are generally formed by dry etching or cleaving. The refractive index contrast between GaN and air is approximately 1.5, giving a reflectivity of approximately 18% for an uncoated facet. High-reflectivity dielectric distributed Bragg reflector (DBR) mirror stacks can be applied to one or both facets to increase reflectivity and reduce mirror loss and lasing threshold. High-reflectivity mirror stacks in conjunction with anti-reflective mirror stacks can also be used for high-power applications to increase slope efficiency. Dielectric coatings (such as SiO_2 and Ta_2O_5) are commonly used for these coatings due to their ease of deposition, high index contrast, and low absorption. Additionally, mirror coatings appear to protect the LD facets from degradation effects related to oxidation (Schoedl *et al.*, 2005).

Early GaN LDs used etched facets since some foreign substrate materials may prohibit cleaving (Sink, 2000). Etched facets are still used on semipolar planes which do not have a cleavable facet along the preferred waveguide orientation (see Section 2). They may also be used for quick feedback of device characteristics since etched facet formation only requires a lithography step and does not require thinning or scribing as for cleaved facets. Etched facets may also allow fabrication of a high density of multiple length laser bars on a single substrate, such as for the variable length stripe method for measuring gain (Farrell, 2010).

Compared to other III–V semiconductors, GaN is a chemically inert material, which makes it relatively resistant to chemical etching and wet-etching techniques (Vartuli *et al.*, 1997). Multiple dry-etching techniques have been investigated over the years, including reactive ion etching (RIE), electron cyclotron resonance etching, magnetron reactive ion etching, inductively coupled plasma etching (ICP), and chemically assisted ion-beam etching (CAIBE) chemically assisted ion-beam etching. Standard Cl_2-based plasma etch conditions for GaN often lead to rough, non-vertical sidewalls. For forming laser facets, this can significantly reduce mirror reflectivity, thereby increasing mirror loss and lasing thresholds, and have an adverse effect on the far-field pattern. In addition, dry etching can lead to ion-induced damage of the etched material, reducing surface

quality and conductivity (Ren *et al.*, 1997). Nearly-vertical etched facets have been demonstrated on *c*-plane GaN using a two-step ICP and wet-etch process (Miller *et al.*, 2009). Smooth facets on *m*-plane GaN were demonstrated with an RIE dry etch using bilayer photoresist mask (Farrell, 2010). Semipolar GaN shows anisotropy of the etch behavior for opposite facets, attributed to the anisotropy of the surface energy of these planes; although this effect may be mitigated with increased bias voltage during the plasma etch (Rass *et al.*, 2010a).

Cleaved facets are preferred because an ideal cleave can provide a crystallographic smooth surface perpendicular to the lasing cavity. However, cleaving can be difficult, even for crystal orientations in which a vertical cleavage plane exists may not be particularly easy to cleave. In these cases, cleaving generally involves lapping and thinning the substrate, scribing, or skip scribing between the waveguides and performing a controlled fracture. For early *c*-plane LDs, the choice of cleaved-facet orientation was limited by the cleavability of the substrate. For example, sapphire substrates cleave along the $(1\bar{1}02)$ *r*-face to form facets on the $(11\bar{2}0)$ *a*-face of GaN. LDs grown on bulk *c*-plane substrates are often cleaved along the *m*-plane $(10\bar{1}0)$ due to the relative ease of cleaving in this direction, and resulting smooth vertical facets. LDs on nonpolar *m*-plane GaN can form smooth cleaved facets along the *a*- or *c*-direction, but the preferred stripe orientation for gain is along the *c*-direction, as explained earlier in Section 2.4. Facets for this preferred orientation on *m*-plane are slightly more difficult to cleave, due to additional bond strength present along the polar axis of the crystal; however, *m*-plane LD facets with an RMS roughness less than 1 nm have been demonstrated (Rass *et al.*, 2010a). The preferred stripe orientation for semipolar $(20\bar{2}1)$ LDs, the $[\bar{1}014]$ direction, does not have an obvious cleavage plane; however, Sumitomo reports cleaved facets for their $(20\bar{2}1)$ LDs (Yoshizumi *et al.*, 2009), suggesting an alternate cleavage plane is available.

Many groups have observed facet or mirror degradation of GaN LDs, which can be responsible for reducing lifetimes, reducing output power, and increasing threshold current with device aging. COD is caused by a sudden increase of temperature at the facet, followed by melting. The threshold for COD is around $40\,\mathrm{mW/cm^2}$ (Takeya *et al.*, 2005) approximately an order of magnitude higher than for GaAs devices (Perlin *et al.*, 2010). COD may be suppressed by widening the optical mode in the transverse and lateral directions, which can be accomplished with wide ridges to encourage multiple lateral modes. Other techniques include reducing optical absorption near the facets using epitaxially formed window structures (Kawaguchi *et al.*, 2010) or reducing recombination near the facets with current-injection free regions (Tomiya *et al.*, 2010). Clever design of facet coatings, such as AlON (Kamikawa *et al.*, 2009) may also help prevent COD. Another source of mirror degradation may be due to

the formation of carbon deposits on the mirror surface, which can limit the device lifetime to less than hundreds of hours (Perlin *et al.*, 2010). The exact cause and mechanism of this form of degradation is the source of ongoing research but seems to be influenced by the presence of nitrogen and gold packaging material.

4.5. Summary

GaN LD performance is highly dependent on waveguide design. Achieving high optical mode overlap with the active region can be challenging from a growth perspective, especially for high-wavelength applications that require high compositions of InGaN in the QW or significant amounts of AlGaN in the surrounding cladding material. Further, large lattice mismatch between AlGaN, InGaN, and GaN layers can cause thick, high-composition ternary alloys to relax which can have deleterious effects on device performance. Mg-doped p-GaN can be a significant source of optical loss as well. This loss may be somewhat mitigated by reducing doping levels (although this may eventually hinder hole transport) or reducing overlap with the upper p-doped waveguiding and cladding materials with improved waveguiding.

Taking advantage of the ability to grow thick QW on nonpolar GaN, low-threshold *m*-plane LDs in the violet and blue spectrum have been demonstrated using a simplified AlGaN-cladding-free waveguide. This elegant design offers reduced growth times while avoiding the disadvantageous consequences of AlGaN growth. Semipolar LDs may also benefit from similar design due to reduced QCSE compared to *c*-plane. For high-wavelength applications, nonpolar and semipolar LDs may require more complicated waveguide designs to ensure adequate waveguiding and avoid relaxation mechanisms that can negatively influence device performance.

5. CONCLUSIONS

GaN is a versatile material system. The inherent asymmetry and polar nature of the wurtzite crystal structure can be a benefit or a disadvantage depending on the application. The additional piezoelectric polarization at an AlGaN/GaN interface on basal *c*-plane GaN, for example, can form a two-dimensional electron gas (2DEG) with sheet charge concentrations an order of magnitude higher than conventional III–V systems, a big advantage for GaN-based electronic applications such as high electron mobility transistors (HEMTs). With a direct, wide bandgap, InGaN-based light emitters have already made a huge impact in the solid-state lighting industry. However, LD development on basal *c*-plane orientation GaN

has been limited by the strong polarization discontinuities between the InGaN QWs and surrounding layers. The reduction in radiative efficiency and blue-shift in wavelength due to QCSE worsens for high In composition QWs required for high-wavelength applications. The nonpolar and semipolar orientations of GaN benefit from eliminated or reduced polarization effects, leading to higher radiative efficiencies and higher anisotropic material gain. Development LDs on these alternate planes gained a lot of momentum once native bulk nonpolar and semipolar substrates became available, and the benefits of these nonbasal planes soon led to competitive device results for both LEDs and LDs in the violet, blue, and green wavelengths.

These alternate nonbasal crystal planes have their own set of challenges. For example, there are limits on indium incorporation, as in the case for nonpolar *m*-plane GaN, or propensity for ternary film relaxation, as in the case for semipolar GaN. Despite these materials challenges however, device performance on nonbasal crystal planes already meet or exceed those of state-of-the-art *c*-plane LDs. Although nonpolar GaN may be limited to wavelengths below 500nm (to date) for reasons related to InGaN QW growth, strong performance of *m*-plane LDs in the violet and blue regions have been demonstrated and further improvements are expected over the next few years with increased development and substrate availability. Although semipolar GaN LDs designs may be limited by strain relaxation limits for waveguiding and cladding layers as described in Section 3, and facet formation described in Section 4, this family of planes has already shown highly competitive results for wavelengths above 500nm. Eventually, nonpolar and semipolar GaN may prove to be the crystal plane of choice to meet the high demands for high performance direct-emission LDs in the blue, green, and into the yellow spectrum.

REFERENCES

Adachi, M., Yoshizumi, Y., *et al*. (2010). *Appl. Phys. Express* **3**(12), 121001.
Asano, T., Tojyo, T., *et al*. (2003). *IEEE J. Quantum Electron.* **39**(1), 135–140.
Asano, T., Yanashima, K., *et al*. (1999). *Phys. Status Solidi (A)* **176**(1), 23–30.
Avramescu, A., Lermer, T., *et al*. (2009). *Appl. Phys. Lett.* **95**(7), 071103.
Avramescu, A., Lermer, T., *et al*. (2010). *Appl. Phys. Express* **3**(6), 061003.
Baker, T. J., Haskell, B. A., *et al*. (2005). *Jpn. J. Appl. Phys.* **44**(29), L920–L922.
Bhattacharyya, J., Ghosh, S., *et al*. (2008). *Appl. Phys. Lett.* **93**(5), 051913.
Chakraborty, A., Baker, T. J., *et al*. (2005a). *Jpn. J. Appl. Phys.* **44**(30), L945–L947.
Chakraborty, A., Haskell, B. A., *et al*. (2005b). *Jpn. J. Appl. Phys.* **44,** L173.
Chen, C., Adivarahan, V., *et al*. (2003). *Jpn. J. Appl. Phys.* **42**(Part 2, No. 9A/B), L1039–L1040.
Chichibu, S. (1996). *Appl. Phys. Lett.* **69**(27), 4188.
Chichibu, S. F., Yamaguchi, H., *et al*. (2008). *Appl. Phys. Lett.* **92**(9), 091912.
Craven, M., Lim, S., *et al*. (2002). *Appl. Phys. Lett.* **81**(3), 469.

De Mierry, P., Guehne, T., *et al*. (2009). *Jpn. J. Appl. Phys.* **48**(3), 031002.
DenBaars, S. P., and Keller, S. (1997). *In* ''Semiconductors and Semimetals,'' (I. P. Jacques and D. M. Theodore, eds.), pp. 11–37. Elsevier, New York 50.
Dingle, R., Shaklee, K. L., *et al*. (1971). *Appl. Phys. Lett.* **19**(1), 5–7.
Domen, K., Horino, K., *et al*. (1997). *Appl. Phys. Lett.* **71**(14), 1996–1998.
Dorsaz, J., Castiglia, A., *et al*. (2010). *Appl. Phys. Express* **3**(9), 092102.
Dwiliński, R., Doradziński, R., *et al*. (2009). *J. Cryst. Growth* **311**(10), 3015–3018.
Enya, Y., Yoshizumi, Y., *et al*. (2009). *Appl. Phys. Express* **2,** 082101.
Farrell, R. M. (2010). *Electrical and Computer Engineering.* University of California, Santa Barbara Doctor of Philosophy.
Farrell, R. M., Feezell, D. F., *et al*. (2007). *Jpn. J. Appl. Phys.* **46**(32), L761–L763.
Farrell, R. M., Haeger, D. A., *et al*. (2010a). *Appl. Phys. Lett.* **96**(23), 231907.
Farrell, R. M., Haeger, D. A., *et al*. (2011). *Appl. Phys. Express* **4**(9), 092105.
Farrell, R. M., Hsu, P. S., *et al*. (2010b). *Appl. Phys. Lett.* **96**(23), 231113.
Feezell, D. F., Schmidt, M. C., *et al*. (2007). *Jpn. J. Appl. Phys* **46**(4), L284–L286.
Fischer, A. M., Wu, Z., *et al*. (2009). *Appl. Phys. Express* **2,** 041002.
Fujito, K., Kubo, S., *et al*. (2009). *MRS Bull.* **34,** 313–317.
Funato, M., Kaneta, A., *et al*. (2010). *Appl. Phys. Express* **3**(2), 021002.
Funato, M., Ueda, M., *et al*. (2006). *Jpn. J. Appl. Phys* **45**(26), L659–L662.
Gardner, N. F., Kim, J. C., *et al*. (2005). *Appl. Phys. Lett.* **86**(11), 111101.
Ghosh, S., Waltereit, P., *et al*. (2002). *Phys. Rev. B* **65**(7), 075202.
Grahn, H. T. (2009). *MRS Bull.* **34**(05), 341–347.
Grzegory, I., and Porowski, S. (2000). *Thin Solid Films* **367**(1–2), 281–289.
Hardy, M. T., Farrell, R. M., *et al*. (2011). *Phys. Status Solidi C* **8**(7–8), 2226–2228.
Haskell, B. A., Baker, T. J., *et al*. (2005). *Appl. Phys. Lett.* **86**(11), 111917.
Haskell, B. A., Wu, F., *et al*. (2003). *Appl. Phys. Lett.* **83**(8), 1554–1556.
Hearne, S. J., Han, J., *et al*. (2000). *Appl. Phys. Lett.* **76**(12), 1534–1536.
Hirai, A., Jia, Z., *et al*. (2007). *Appl. Phys. Lett.* **91**(19), 191906.
Hsu, P. S., Kelchner, K. M., *et al*. (2010). *Appl. Phys. Express* **3**(5), 052702.
Hsu, P. S., Young, E. C., *et al*. (2011). *Appl. Phys. Lett.* **99**(8), 081912.
Huang, C.-Y., Lin, Y.-D., *et al*. (2010a). *J. Appl. Phys.* **107**(2), 023101.
Huang, C.-Y., Tyagi, A., *et al*. (2010b). *Jpn. J. Appl. Phys.* **49**(1), 010207.
Im, J. S., Kollmer, H., *et al*. (1998). *Phys. Rev. B* **57**(16), R9435–R9438.
Ito, S., Yamasaki, Y., *et al*. (2004). *Jpn. J. Appl. Phys.* **43**(1), 96–99.
Jang, H. W., Baik, J. M., *et al*. (2004). *J. Electrochem. Soc.* **151**(8), G536.
Kamikawa, T., Kawaguchi, Y., *et al*. (2009). *Appl. Phys. Lett.* **95**(3), 031106.
Kamiyama, S., Honshio, A., *et al*. (2005). *Phys. Status Solidi C* **2**(7), 2121–2124.
Kawaguchi, M., Kasugai, H., *et al*. (2010). IEEE Int. Semicond. Laser Conf. 22nd, pp. 26–30.
Kelchner, K. M. (2012). *Nonpolar Blue Laser Diodes by MOCVD. Electrical and Computer Engineering.* University of California, Santa Barbara Doctor of Philosophy.
Kelchner, K. M., Farrell, R. M., *et al*. (2010). *Appl. Phys. Express* **3**(9), 092103.
Kelchner, K. M., Lin, Y.-D., *et al*. (2009). *Appl. Phys. Express* **2,** 071003.
Kim, Y. S., Kaneta, A., *et al*. (2011). *Appl. Phys. Express* **4**(5), 052103.
Kim, K.-C., Schmidt, M. C., *et al*. (2007a). *Appl. Phys. Lett.* **91**(18), 181120.
Kim, K.-C., Schmidt, M. C., *et al*. (2007b). *Phys. Status Solidi RRL* **1**(3), 125–127.
Kioupakis, E., Rinke, P., *et al*. (2010a). *Phys. Rev. B* **81**(24), 241201(R).
Kioupakis, E., Rinke, P., *et al*. (2010b). *Appl. Phys. Express* **3**(8), 082101.
Kisin, M. V., Brown, R. G. W., *et al*. (2009). *Appl. Phys. Lett.* **94**(2), 021108.
Kneissl, M., Bour, D. P., *et al*. (1999). *Appl. Phys. Lett.* **75**(4), 581–583.
Kojima, K., Kamon, H., *et al*. (2008). *Phys. Status Solidi C* **5**(9), 3038–3041.
Kojima, K., Schwarz, U. T., *et al*. (2007a). *Opt. Express* **15**(12), 7730–7736.
Kubota, M., Okamoto, K., *et al*. (2008). *Appl. Phys. Express* **1**(1), 011102.

Kucharski, R., Rudziński, M., *et al*. (2009). *Appl. Phys. Lett.* **95**(13), 131119.
Kuramoto, M., Sasaoka, C., *et al*. (2002). *Phys. Status Solidi* **A192**(2), 329–334.
Kyono, T., Yoshizumi, Y., *et al*. (2010). *Appl. Phys. Express* **3**(1), 011003.
Lermer, T., Schillgalies, M., *et al*. (2010). *Phys. Status Solidi A* **207**(6), 1328–1331.
Lin, Y.-D., Chakraborty, A., *et al*. (2009a). *Appl. Phys. Lett.* **94**(26), 261108.
Lin, Y.-D., Hardy, M. T., *et al*. (2009b). *Appl. Phys. Express* **2,** 082102.
Lin, Y.-D., Huang, C.-Y., *et al*. (2009c). *Appl. Phys. Lett.* **95**(8), 081110.
Lin, Y.-D., Yamamoto, S., *et al*. (2010). *Appl. Phys. Express* **3**(8), 082001.
Ling, S.-C., Lu, T.-C., *et al*. (2010). *Appl. Phys. Lett.* **96**(23), 231101.
Lutgen, S., Avramescu, A., *et al*. (2010). *Phys. Status Solidi A* **207**(6), 1318–1322.
Lutgen, S., Dini, D., *et al*. (2011). *Proc. SPIE* **7953**, 79530G-1.
Masui, H., Chakraborty, A., *et al*. (2005). *Jpn. J. Appl. Phys.* **44**(43), L1329–L1332.
Matthews, J. W., and Blakeslee, A. E. (1974). *J. Cryst. Growth* **27,** 118–125.
Miller, M. A., Crawford, M. H., *et al*. (2009). *J. Electron. Mater.* **38**(4), 533–537.
Miyajima, T., Yoshida, H., *et al*. (2001). *Mater. Sci. Eng. B* **82**(1–3), 248–252.
Miyoshi, T., Masui, S., *et al*. (2010). *Phys. Status Solidi A* **207**(6), 1389–1392.
Miyoshi, T., Yanamoto, T., *et al*. (2008). *Proc. SPIE* **6894**. 689414-1.
Morkoc, H., Hamdani, F., *et al*. (1998). Semiconductors and Semimetals Vol. 50, p. 193. Academic Press Inc., London/New York.
Müller, J., Brüderl, G., *et al*. (2010). *Proc. SPIE* **7602**(1), 760222.
Nakamura, S., Pearton, S. J., *et al*. (2000). The Blue Laser Diode: The Complete Story. 2nd ed. Springer, Berlin Heidelberg.
Nakamura, S., Senoh, M., *et al*. (1996). *Jpn. J. Appl. Phys. Part 2* **35**(1B), L74–L76.
Nakamura, S., Senoh, M., *et al*. (1997). *Jpn. J. Appl. Phys. Part 2* **36**(8B), L1059–L1061.
Nam, O. H., Ha, K. H., *et al*. (2006). *Proc. SPIE* **6133**(1), 61330N-1.
Neugebauer, J., and Van de Walle, C. G. (1999). *J. Appl. Phys.* **85**(5), 3003–3005.
Nichia (2007). Nichia starts engineering sample shipments of 1W CW pure blue semiconductor. [Press release]. Retrieved from:http://www.nichia.co.jp/en/about_nichia/2007/2007_112001.html.
Nichia (2010). Nichia starts shipments of green semiconductor laser. [Press release]. Retrieved from:http://www.nichia.com/en/about_nichia/2010/2010_070701.html.
Nishizuka, K., Funato, M., *et al*. (2004). *Appl. Phys. Lett.* **85**(15), 3122.
Niwa, A. (1997). *Appl. Phys. Lett.* **70**(16), 2159.
Northrup, J. E., and Neugebauer, J. (1999). *Phys. Rev. B* **60**(12), R8473.
Okamoto, K., Kashiwagi, J., *et al*. (2009). *Appl. Phys. Lett.* **94**(7), 071105.
Okamoto, K., Ohta, H., *et al*. (2007a). *Jpn. J. Appl. Phys.* **46**(No. 9), L187–L189.
Okamoto, K., Tanaka, T., *et al*. (2007b). *Jpn. J. Appl. Phys.* **46**(No. 35), L820–L822.
Okamoto, K., Tanaka, T., *et al*. (2008). *Appl. Phys. Express* **1,** 072201.
Optics.org (2010). Osram set for green diode ramp in 2012. Retrieved from:http://optics.org/news/1/7/17.
Perlin, P., Marona, L., *et al*. (2010). *Proc. IEEE* **98**(7), 1214–1219.
Peter, M., Laubsch, A., *et al*. (2008). *Phys. Status Solidi C* **5**(6), 2050–2052.
Pioneer (2010). Pionner ships first BDXL computer drive to read and wrte new Blu-Ray disc recording Format. [Press release]. Retrieved from:http://www.pioneerelectronics.com/PUSA/Press-Room/Pioneer+-Ships+First+BDXL+Computer+Drive+to+Read+and+Write+New+Blu-ray+Disc+Recording+Format.
Queren, D., Avramescu, A., *et al*. (2009). *Appl. Phys. Lett.* **94**(8), 081119.
Queren, D., Schillgalies, M., *et al*. (2009). *J. Cryst. Growth* **311**(10), 2933–2936.
Raring, J. W., Schmidt, M. C., *et al*. (2010). *Appl. Phys. Express* **3**(11), 112101.
Rass, J., Wernicke, T., *et al*. (2010a). *Phys. Status Solidi A* **207**(6), 1361–1364.
Rass, J., Wernicke, T., *et al*. (2010b). *Phys. Status Solidi RRL* **4**(1–2), 1–3.

Ren, F., Lothian, J., *et al*. (1997). *J. Electron. Mater.* **26**(11), 1287–1291.
Romanov, A. E., Baker, T. J., *et al*. (2006). *J. Appl. Phys.* **100**(2), 023522.
Romanov, A. E., Young, E. C., *et al*. (2011). *J. Appl. Phys.* **109**(10), 103522.
Ryu, H. Y., Ha, K. H., *et al*. (2009). *J. Appl. Phys.* **105**(10), 103102.
Sala, F. D., Di Carlo, A., *et al*. (1999). *Appl. Phys. Lett.* **74**(14), 2002–2004.
Sato, H., Chung, R. B., *et al*. (2008). *Appl. Phys. Lett.* **92**(22), 221110.
Schade, L., Schwarz, U. T., *et al*. (2011). *Phys. Status Solidi B* **248**(3), 638–646.
Scheibenzuber, W., Schwarz, U., *et al*. (2009). *Phys. Rev. B* **80**(11), 115320-1.
Schmidt, M. C., Kim, K.-C., *et al*. (2007a). *Jpn. J. Appl. Phys. Part 2* **46**(8–11), L190–L191.
Schmidt, M. C., Kim, K.-C., *et al*. (2007b). *Jpn. J. Appl. Phys.* **46**(7), L126–L128.
Schoedl, T., Schwarz, U. T., *et al*. (2005). *J. Appl. Phys.* **97**(12), 123102.
Schwarz, U. T., Braun, H., *et al*. (2007). *Proc. SPIE.* **6485,** 648506-1.
Schwarz, U. T., Pindl, M., *et al*. (2005). *Phys. Status Solidi A* **202**(2), 261–270.
Semiconductor Today (2010). Green laser diode market $500m by 2016 as pico-projector market drives growth. Retrieved from:http://www.semiconductor-today.com/news_items/2010/APRIL/YOLE_140410.htm.
Sharma, R., Pattison, P. M., *et al*. (2005). *Appl. Phys. Lett.* **87**(23), 231110.
Shokhovets, S., Goldhahn, R., *et al*. (2003). *J. Appl. Phys.* **94**(1), 307.
Sink, R. K. (2000). *Electrical and Computer Engineering*. University of California, Santa Barbara Doctor of Philosophy: 236.
Sizov, D., Bhat, R., *et al*. (2011). *Appl. Phys. Lett.* **99**(4), 041117.
Speck, J. S., and Chichibu, S. F. (2009). *MRS Bull.* **34**(05), 304–312.
Srinivasan, S., Geng, L., *et al*. (2003). *Appl. Phys. Lett.* **83**(25), 5187.
Strauss, U., Brüninghoff, S., *et al*. (2008a). *Proc. SPIE* **6894**, 689417-1.
Strauss, U., Eichler, C., *et al*. (2008b). *Phys. Status Solidi C* **5**(6), 2077–2079.
Sumitomo (2010). Sumitomo Electric Announces Large Scale Production of the World's First 2-inch Semipolar/Nonpolar GaN Substrates for Green Lasers. [Press release] Retrieved from:http://global-sei.com/news/press/10/10_25.html.
Sun, Y. J., Brandt, O., *et al*. (2003). *Phys. Status Solidi B* **240**(2), 360–363.
Takeuchi, T., Amano, H., *et al*. (2000). *Jpn. J. Appl. Phys.* **39,** 413.
Takeya, M., Hashizu, T., and Ikeda, M. (2005). *Proc. SPIE* **5738,** 63–71.
Takeya, M., Yanashima, K., *et al*. (2000). *J. Cryst. Growth* **221,** 646–651.
Tokunaga, H., Fukuda, Y., *et al*. (2008). *Phys. Status Solidi C* **5**(9), 3017–3019.
Tomiya, S., Goto, O., *et al*. (2010). *Proc. IEEE* **98**(7), 1208–1213.
Tsuda, Y., Ohta, M., *et al*. (2008). *Appl. Phys. Express* **1**(1), 011104.
Tyagi, A., Farrell, R. M., *et al*. (2010). *Appl. Phys. Express* **3**(1), 011002.
Tyagi, A., Lin, Y.-D., *et al*. (2008). *Appl. Phys. Express* **1,** 091103.
Tyagi, A., Wu, F., *et al*. (2009). *Appl. Phys. Lett.* **95**(25), 251905.
Tyagi, A., Zhong, H., *et al*. (2007). *Jpn. J. Appl. Phys.* **46**(19), L444–L445.
Uchida, S., Takeya, M., *et al*. (2003). *Sel. Top. IEEE J. Quantum Electron.* **9**(5), 1252–1259.
Ueda, M., Funato, M., *et al*. (2008). *Phys. Rev. B* **78**(23), 233303.
Ueno, M., Yoshizumi, Y., *et al*. (2011). *J. Cryst. Growth* **315**(1), 258–262.
Van de Walle, C. G., and Neugebauer, J. (2004). *J. Appl. Phys.* **95**(8), 3851–3879.
Vartuli, C. B., Pearton, S. J., *et al*. (1997). *Solid State Electron.* **41**(12), 1947–1951.
Waltereit, P., Brandt, O., *et al*. (2007). *Nature* **406,** 865–868.
Wu, F., Lin, Y.-D., *et al*. (2010). *Appl. Phys. Lett.* **96**(23), 231912.
Wunderer, T., Hertkorn, J., *et al*. (2008). *Proc. SPIE.* **6894,** 68940V.
Yamada, H., Iso, K., *et al*. (2008a). *Phys. Status Solidi RRL* **2**(2), 89–91.
Yamada, H., Iso, K., *et al*. (2008b). *Appl. Phys. Express* **1,** 041101.
Yan, Q., Rinke, P., *et al*. (2010). *Appl. Phys. Lett.* **97**(18), 181102.
Yoshida, S., Yokogawa, T., *et al*. (2011). *Appl. Phys. Lett.* **99**(13), 131909.
Yoshizumi, Y., Adachi, M., *et al*. (2009). *Appl. Phys. Express* **2**(9), 092101.

Young, E. C., Gallinat, C. S., *et al*. (2010a). *Appl. Phys. Express* **3**(11), 111002.
Young, E. C., Romanov, A. E., *et al*. (2011). *Appl. Phys. Express* **4**(6), 061001.
Young, E. C., Wu, F., *et al*. (2010b). *Appl. Phys. Express* **3**(1), 011004.
Zhang, M., Banerjee, A., *et al*. (2011). *Appl. Phys. Lett*. **98**(22), 221104.
Zhang, L. Q., Jiang, D. S., *et al*. (2009). *J. Appl. Phys.* **105**(2), 023104.
Zhao, Y., Tanaka, S., *et al*. (2011). *Appl. Phys. Express* **4**(8), 082104.